Accepted Manuscript

Geological Society, London, Special Publications

A new depositional model for the Tuaheni Landslide Complex, Hikurangi Margin, New Zealand

Benjamin Couvin, Aggeliki Georgiopoulou, Joshu J. Mountjoy, Lawrence Amy, Gareth J. Crutchley, Morgane Brunet, Sebastian Cardona, Felix Gross, Christoph Böttner, Sebastian Krastel & Ingo Pecher

DOI: https://doi.org/10.1144/SP500-2019-180

Received 30 September 2019
Revised 22 November 2019
Accepted 26 November 2019

A new depositional model for the Tuaheni Landslide Complex, Hikurangi Margin, New Zealand

Abbreviated title: TUAHENI LANDSLIDE DEPOSITIONAL MODEL

BENJAMIN COUVIN[1*], AGGELIKI GEORGIOPOULOU[2], JOSHU J. MOUNTJOY[3], LAWRENCE AMY[1], GARETH J. CRUTCHLEY[4], MORGANE BRUNET[5], SEBASTIAN CARDONA[6], FELIX GROSS[7], CHRISTOPH BÖTTNER[4], SEBASTIAN KRASTEL[7] AND INGO PECHER[8]

[1]*Irish Centre for Research in Applied Geosciences, University College Dublin, Ireland*

[2]*School of Environment and Technology, University of Brighton, United Kingdom*

[3]*National Institute for Water and Atmospheric Research, Wellington, New Zealand*

[4]*GEOMAR Helmholtz-Zentrum für Ozeanforschung, Kiel, Germany*

[5]*Géosciences Rennes, Université Rennes 1, France*

[6]*Colorado School Of Mines, Golden, CO, United States of America*

[7]*Institute of Geosciences, University of Kiel, Germany*

[8]*School of Environment, University of Auckland, New Zealand*

*Corresponding author: B. Couvin (benjamin.couvin@ucdconnect.ie)

Abstract: The Tuaheni Landslide Complex (TLC) is characterised by areas of compression upslope and extension downslope. It has been thought to consist of a stack of two genetically linked landslide units identified on seismic data. We use 3D seismic reflection, bathymetry data, and IODP core U1517C (Expedition 372), to understand the internal structures, deformation mechanisms and depositional processes of the TLC deposits. Unit II and Unit III of U1517C correspond to the two chaotic units in 3D seismic data. In the core, Unit II shows deformation whereas Unit III appears more like an *in situ* sequence. Variance attribute analysis shows that Unit II is split in lobes around a coherent stratified central ridge and is bounded by scarps. By contrast, we find that Unit III is continuous beneath the central ridge and has an upslope geometry that we interpret as a channel-levee system. Both units show evidence of lateral spreading due to the presence of the Tuaheni Canyon removing support from the toe. Our results suggest that Unit II and Unit III are not genetically linked, that they are separated substantially in time and they had different emplacement mechanisms, but fail under similar circumstances.

Subaqueous landslides have long been recognised as a geohazard. They can trigger tsunamis, endanger offshore installations and may induce coastal subsidence (Hampton 1996; Mulder & Cochonat 1996; Talling 2013; Fruergaard *et al.* 2015). Some events like the 1929 Grand Banks earthquake off Newfoundland (Piper *et al.* 1999) or the more recent Nice airport collapse in 1979 (Ioualalen 2010; Kelner *et al.* 2016) are examples of cases where human settlements and installations have been directly impacted by subaqueous landslides. Considering the significance of

this implication, it is important to better constrain the mechanisms that can lead to the generation and reactivation of subaqueous landslides.

At the Hikurangi Margin, off the eastern coast of New Zealand's North Island, the Tuaheni Landslide Complex (TLC) (Fig. 1) has been interpreted from bathymetry data analysis as a slow-moving landslide (Mountjoy *et al.* 2009). The landslide was recognised from its surface roughness on bathymetry data, while its creeping movement was interpreted on the basis of a reactivated landslide morphology, including a downslope extensional domain, arcuate (concave from downslope) surface scarps and strike-slip faulting along the margins of the landslide body (Mountjoy *et al.* 2009).

Recognition of MTDs in seismic data is generally based on the identification of a disrupted or chaotic seismic facies underlain by a basal shear surface (Bull *et al.* 2009). The TLC is thought to be composed of two or more stacked landslide units (Mountjoy *et al.* 2014; Gross *et al.* 2018; Böttner *et al.* 2018; Kuhlmann *et al.* 2018). In 2017, during IODP Expedition 372 (Exp 372), a 190 m core (U1517C) was retrieved at the TLC (Pecher *et al.* 2018) (Fig. 1b). Physical properties were also acquired during Exp 372, such as density, velocity, magnetic susceptibility and gamma-ray. These data helped correlate the unit boundaries of core U1517C with reflectors in seismic data (Pecher *et al.* 2018), but they are not used further in this study.

Initial observations of the core highlighted a discrepancy between the observed lithology and the seismic facies, as the deposits above what should be the base of slide at 66 mbsf appear largely undeformed and were therefore interpreted as a remobilised intact block (Pecher *et al.* 2018). This interpretation seems to clash with the previous model of a stack of distinct chaotically mixed landslide events without blocks (Böttner *et al.* 2018; Gross *et al.* 2018). Hence, an integrated approach was taken in this study for a better characterisation of the TLC morphology and depositional history.

In this study we analyse the sedimentary character and depositional environment of the TLC by integrating three-dimensional (3D) seismic data with the newly acquired sedimentological information from core U1517C. Our aims are to test the hypothesis that the lower landslide unit is actually an *in situ* sedimentary package despite having the seismic characteristics of a MTD to determine from seismic data analysis a most likely depositional history of the TLC.

Geological setting

The Hikurangi Margin is located off the east coast of the North Island, New Zealand, and is an active subduction zone where the Pacific Plate is subducting beneath the Australian Plate at an average rate of ~ 4-5 cm yr^{-1} relative to the Australian Plate (Anderson & Webb 1994; Wallace *et al.* 2004). The study area is located on the upper continental slope, which is underlain by a Quaternary succession of sea-level controlled sedimentary units with clinoform geometry (Pedley *et al.* 2010; Mountjoy *et al.* 2009). Rapid tectonic deformation and eustasy have been significant in controlling sediment flux and shifting depocenters on the Hikurangi margin (Paquet *et al.* 2009). However, higher sediment accumulation rates have been found particularly associated with climato-eustatic extremes, correlating with high terrestrial erosion (Paquet *et al.* 2009). The TLC mass consists of failed clinoform material from the upper slope (Mountjoy *et al.* 2009).

In terms of oceanic currents, the zone of study is located within a large zone of mixing where the northward Wairarapa Eddy meets the eastward East Cape Current (Chiswell *et al.* 2005). However, very little is known about local deep-water currents at the Tuaheni Slope. Sea level fluctuations were of high amplitude and high frequency during the Quaternary, with sea level variations of 75 to 150 m

in New Zealand (Newnham *et al.* 1999). The sea level rose 120 m since the Last Glacial Maximum (c. 15-25 ka BP) (Wright *et al.* 1995). While South Island was largely covered by ice during the Last Glacial Maximum, North Island had a very limited amount of glaciers (Newnham *et al.* 1999).

The TLC consists of two mass transport complexes, Tuaheni North and Tuaheni South. This study focuses on Tuaheni South, which, for means of simplification, will be referred to as 'the TLC'. The TLC consists of three lobes (from south to north): Lobes T1, T2 and T3. Lobes T2 and T3 are separated by a topographic high (central ridge) (Mountjoy *et al.* 2009) (Fig. 1b). The structural regime within the landslide body is unusual in that it displays a compressional zone upslope and an extensional zone downslope (Mountjoy *et al.* 2009; Mountjoy *et al.* 2014). The extensional part of the TLC downslope overlies a sedimentary sequence deformed by a set of NE-SW striking high dip angle normal faults (Böttner *et al.* 2018).

In previous studies, the TLC was interpreted from seismic data to consist of a stack of at least two MTD units, recognisable from their chaotic facies (Mountjoy *et al.* 2014; Gross *et al.* 2018; Kuhlmann *et al.* 2018). These two units appear in seismic data to be separated by a negative impedance reflection with respect to the seafloor reflector, whose origin remains enigmatic (Gross *et al.* 2018). After considering different geological scenarios for this reflection (referred to in Gross *et al.* (2018) as the 'intra debris reflector'), Gross *et al.* (2018) suggested that it likely represents the basal shear surface of the upper debris unit and possibly a zone of accumulation for excess fluid pressure.

Methods

Seismic and bathymetry data

A high-resolution 3D seismic reflection volume was acquired at the TLC during *RV Tangaroa* cruise TAN1404 in 2014, using a P-Cable System for high-resolution 3D seismic acquisition. The total area covered by the seismic volume is approximately 69 km^2 (Böttner *et al.* 2018; Gross *et al.* 2018) (Fig. 1b). The resolution of the data is circa 5 m horizontal and 2-3 m vertical, with a penetration of up to 750 m (roughly equivalent to 1 s two-way travel time). The reader is referred to Gross *et al.* (2018) for a full description of the acquisition and processing details of the P-Cable data. The bathymetry data were also acquired during the TAN1404 voyage, using a Kongsberg EM302 SWATH multi-beam echo-sounder (Gross *et al.* 2018).

Core logging and lithology

In 2017, a 190 m long sediment core (U1517C) was drilled in the distal part of Lobe T2 of the TLC during Exp 372 (Pecher *et al.* 2018). A recovery of over 90% allowed for a continuous record through the TLC deposit and the base of the slide to the underlying stratigraphy. The core was first bulk described during the expedition and five lithological units were defined (I to V) based on lithological changes as well as magnetic susceptibility logs (Pecher *et al.* 2018). In order to understand better the internal structure of the landslide deposits, we have described and logged Units I, II and III of Core U1517C in more detail. We identified the lithology and sedimentary structures of the units to help constrain a more precise depth and nature of the boundaries between each of the units. We measured grain size in parts of the core within Unit II and Unit III using a Malvern Mastersizer 3000, which helped provide calibration for core-wide grain size determination. 74 samples were measured for Unit II (sections 1H-4W, 2H-3W, 5F-2W, 5F-4W and 6F-1W) and 66 for Unit III (sections 9F-3W, 10F-1W, 10F-2W, 11F-4W, 13F-3W). The samples were chosen so that most lithologies found in the

core are represented. Considering the consistency of the results, only representative samples are shown in this study.

Seismic attributes and interpretation

We used the Petrel 2018 software to visualise and analyse the data. The seismic data were interpreted in two-way travel time. We focused on four major horizons: the Top of Unit II (R1), the Base of Unit II (R2), the Top of Unit III (R3) and the Base of Unit III (R4). The sea floor surface (R0) was also picked and, due to the limitations in vertical seismic resolution, was merged with R1 in most of the central and distal domains of the 3D survey. This is due to Unit I being a surface drape, not covering the top of Unit II uniformly throughout the volume, and therefore only resolvable in the proximal domain where its thickness is greatest. We interpreted the horizons using both manual and automatic picking, and surfaces were created through extrapolation and gridding from the acquired datapoints. Seismic attributes, such as variance, RMS amplitudes, gradient, most negative amplitude and most positive amplitude, were then derived from the 3D seismic volume in order to detect internal deformation, faults, unconformities and deposit geometry. Only the variance and gradient attributes provided results that were useful for this study.

The horizons were interpreted from seismic data according to the following steps:

(1) The bounding surfaces were defined by correlation of the seismic data with stratigraphic information from core U1517C at site U1517;
(2) Units II and III were mapped by picking the bounding surfaces (top and base) throughout the volume (the units themselves were identified as chaotic discontinuous seismic facies or transparent deformed seismic facies);
(3) When the seismic facies changed abruptly laterally into a facies of continuous, parallel reflections, it was considered that a scarp or unit margin was between them.

Results

Unit II

Lithology. From observation in core U1517C, Unit II comprises many sand bodies, with thicknesses ranging between 2 cm and 20 cm. Most of the sand units show evidence of deformation such as folds and injectites, while some of them are abruptly truncated (Fig. 2a). In general, their internal structure is massive and their base is sharp (Fig. 2a). The top of these layers can be either a sharp contact or gradually fining upwards (Fig. 2a). The average observed grain size is very fine sand to fine sand. Grain size measurements show a well sorted very fine sand with a mode at 70 µm (e.g. Fig 2b). The colour of these sands is olive grey (5Y-5/2 on the Munsell scale) (Fig. 2a). In addition to massive sand layers, discontinuous thin sand lenses (< 1 cm thickness/diameter) were observed (Fig. 2a). Similar in colour and grain size to the massive layers, they are often accompanied by shell fragments or reddish-brown specs, likely high in iron.

The rest of the sedimentary sequence consists mostly of structureless clayey silt. The colour of these silts is olive grey (5Y-5/2 on the Munsell scale) (Fig. 2a). Grain size measurements show a poorly sorted sediment ranging from ~ 0.5 to 100 µm with a mode at ~ 8 µm (e.g. Fig 2b). The uppermost 2 m of Unit II are characterised by a colour banding in the silts at 10-20 cm intervals (Fig. 2a).

Seismic character. In seismic reflection data, Unit II is characterised by a chaotic to transparent seismic facies, where any internal reflectors are discontinuous (Fig. 3). In the upslope domain,

northwest of the central ridge, Unit II features large blocks of subparallel reflectors, surrounded by faults (Fig. 3). Unit II is continuous upslope until the headscarp toward the northwest (Figs 3 & 4). In the distal part of Lobe T2, Unit II features normal faults (Fig. 5). In the distal part of Lobe T3, Unit II is faulted by normal and strike-slip faults with an E-W orientation (Fig. 5). Fault interpretation is based primarily on the morphology of the seafloor reflection; it is very difficult or impossible to distinguish fault surfaces within the chaotic units themselves, partly due to migration artefacts arising from strong underlying reflections. North of the central ridge, compression occurs as evidenced by the presence of thrust faults (Fig. 3).

Lateral extent. The lateral margins of the unit are identifiable in seismic data; geographically, they correspond to seafloor scarps that can be seen in bathymetry data (Fig. 1b). The latter have been well described by Mountjoy *et al.* (2009). Upslope, two main head scarps are identified: a 1 km wide amphitheatric one to the west, and a narrower 500 m wide one to the east. Their heights are comparable, c. 300 m, and their maximum evacuated length is about 2 km (Mountjoy *et al.* 2009) (Fig. 6). At the northern margin of Lobe T3, as well as around the central ridge and at the western margin of Lobe T2 (in the distal domain only), the unit is bounded by side scarps (Figs 4, 5 & 6). At the western margin towards the proximal zone, instead of being bounded by a side scarp, the unit extends to the southwest (Lobe T1), ramping down, eroding the stratigraphy directly below, creating a NW-SE oriented extensional ramp (*sensu* Bull *et al.* 2009) (Fig. 6). Unit II has a toe, identifiable in seismic data by the pinching out of the chaotic reflectors (Figs 3a & 3d). At the most downslope extent of the TLC, Lobe T2 is laterally bound by the walls of the Tuaheni Canyon (Fig. 1b).

Boundaries. In core, the top of Unit II corresponds to the base of Unit I, and appears as a smooth progressive boundary from featureless clay above to an alternation of deformed clayey silt layers and deformed fine sand layers downcore (Fig. 2a). At the location where the core was drilled, Unit I is a 3 m thick hemipelagic drape and therefore at the limit of the resolution of the seismic data. For seismic interpretation purposes, it was decided to consider the seafloor as the top of Unit II at that location. Only towards the headscarps of Unit II does Unit I increase in thickness to the degree that it could be mapped separately (Figs 3 & 4). In the core, the basal surface of Unit II is distinctly defined by a 2 cm thick siliciclastic dark grey layer (5Y-4/2 on the Munsell scale – this colour has been found nowhere else within the described portion of the core) at 40.74 m depth. It is massive, structureless, apparently undeformed apart from the coring process, has a sharp top and a sharp base and presents a similar grain size to other layers in Unit II (Fig. 2a). However, the layer appears from direct observation to be more consolidated than the surrounding layers.

This layer corresponds in seismic data to a reflector of negative acoustic impedance (reflector R3). Despite covering a large area, this reflector is not completely continuous throughout the volume. It could nonetheless be picked with a good level of confidence in the largest part of the seismic volume and then interpolated.

Seismic attribute analysis. Seismic attributes were calculated from the seismic volume in an attempt to extract more information about the units' internal character. Variance is a seismic attribute that is generally used to enhance faults, channel and valley margins, prominent changes in dip and lateral discontinuities in general (Randen & Sønneland 2005; Koson *et al.* 2014; Gee & Gawthorpe 2019). A variance map (Fig. 7) of a surface parallel to reflector R3, 20 ms above it, shows a sharp transition from a zone where variance has a consistently high value (that corresponds to a zone of consistently discontinuous or transparent seismic facies), that is to say, the TLC deposits (> 0.4), to a zone of low variance value (where the seismic reflectors are continuous), which corresponds to the undisturbed central ridge and lowstand spur sedimentary sequences (0–0.3) (Fig. 7a).

Unit II is consistently thick in the upslope domain (ranges between 50 and 60 ms thickness) and gets progressively thinner downslope to approximately 20 ms before pinching out (Fig. 8a).
Towards the downslope domain of Lobe T2, a pattern of arcuate ridges appears on thickness data (Fig. 8a). These features are concave in the updip direction and do not extend beyond the margins on Unit II (e.g. the central ridge) (Fig. 8a). On gradient and elevation maps an elongated ridge is also visible on Horizon R2 within Lobe T2 (Fig. 6).

Unit III

Lithology. In core U1517C, the sedimentary succession of Unit III (from 40.74 m to 66.7 m) consists mainly of fine laminae, alternations of silty and clay-rich thin beds. Some of the silt beds contain shell fragments (Fig. 2a). The sand fraction is minimal compared to Unit II. Grain size ranges between ~ 1 and 120 µm (e.g. Fig. 2b). In terms of macrostructures, little deformation is observed, with scarce thin fine sand beds being locally deformed (Fig. 2a).
Seismic character. In seismic data, Unit III is characterised by a chaotic to transparent seismic facies (Figs 3, 4 & 5). At discrete locations of the volume, blocks characterised by a stronger amplitude and a parallel orientation of their reflectors can be observed (Fig. 3). For the same reason as Unit II, it is very difficult to identify faults within the chaotic facies of Unit III. In the upslope domain, we interpret large faults at each side of the thickest part of the unit (Fig. 4). In the central and distal domains, the seismic facies alternate between transparent, chaotic and parallel. However, no major deformation is observed. The unit seems to be continuous under the central ridge (Fig. 5).
Lateral extent. The lateral margins of Unit III are characterised by the absence of side scarps or clearly defined vertically oriented margins (Figs 4 & 5). We observe a smooth lateral seismic facies change or a progressive pinch-out of the chaotic body (Fig. 4 & 5). In addition, unlike Unit II, Unit III does not show evidence of a headscarp. As hinted in previous studies (cf. Fig. 5 in: Gross *et al.* 2018), Unit III seems to be confined within a channel in the most upslope domain (Fig. 4). Our reinterpretation of the dataset revealed a more precise location and morphology of this channel. Within the channel, the unit is thicker (50 to 60 ms) than in the rest of the study area (approx. 20 to 30 ms) (Fig. 8b). At the mouth of the channel in the seaward direction, the unit seems to spread out laterally and form two thin levees or channel wings toward the north and the south respectively, the northern one being more extensive than the southern one. A tributary channel was also identified directly north-northwest of the southern levee (Fig. 9). Unit III has a larger geographical extent than Unit II. It is also continuous under the central ridge and even beyond the side scarps of Unit II (Fig. 9). The extent of Unit III is therefore not bounded by the margins of the TLC as they appear in bathymetry data.
Boundaries. The top surface of Unit III corresponds in core U1517C to the base of the grey layer identified as the base of Unit II, described above, and presumed to correspond in seismic data to the R3 Reflector.
The base of Unit III is identified in seismic data as a reflector of negative acoustic impedance. In core U1517C, the base of Unit III was defined at 66.7 m depth based on lithological changes as well as magnetic susceptibility logs (Pecher *et al.* 2018) (Fig. 2a). However, during our visual observations of the core, no obvious basal shear surface could be identified at this depth.
Seismic attribute analysis. The gradient map of the base of Unit III shows a surface with terraces and steps: the surface is rather flat except for discrete locations where the relative gradient is increased locally (Fig. 9c & 9d). Moreover, variance data show some isolated round patches throughout the volume (Fig. 7b). These patches have a lower variance value (< 0.3) (Fig. 7b). The density of these

lower variance patches within this slice (Fig. 7b) is approximately 35%, and their size ranges from 5 m to 500 m in diameter. We interpret from variance attribute analysis that Unit III is not laterally bound by the central ridge (Fig. 7b), as the characteristic low-variance response of the central ridge deposits does not appear on variance results for Unit III.

Central ridge

In seismic data, the central ridge deposits present a parallel continuous to transparent facies (Fig. 5). Overlying Unit III, the reflectors form a wedge that is thickest in its central part (up to 160 ms). The reflectors appear to be truncated by faults. It is surrounded by Unit II debris at its north, south and west sides. Variance data shows that the central ridge has a low variance value (< 0.3) (Fig. 7a). In its northermost part, the central ridge is overlain by small blocks of chaotic facies (Fig. 6), which are arguably part of Unit II.

Discussion

Interpretation of the TLC units' lithology and deposition mechanisms will be discussed following order of emplacement, thus starting with the oldest unit.

Unit III emplacement model

From interpretation of seismic data and geometric attributes such as variance and gradient, Unit III seems to have significantly different characteristics from Unit II. A key interpretation that we have made in this re-evaluation of the data is that Unit III is continuous beneath the central ridge (Fig. 5). We base this interpretation on a re-mapping of the reflector that separates Unit II and Unit III (the intra-debris reflector, as defined by Gross *et al.* 2018), with the added constraint of sediment character at IODP Site U1517A. We are confident that this reflector (here referred to as reflector R3) can be picked beneath the central ridge (Fig. 5). An important factor to test for our new interpretation is the consistency of the Unit III seismic facies both beneath the central ridge and beneath Unit II.

Unit III upslope seems to present an erosive base as it creates a channel that cuts through the previously deposited units (Fig. 4). The fill of this channel extends on either side of the channel bed, in a geometry that resembles tapered wedges: a feature usually associated with channel-levee systems and deep sea fans (Babonneau *et al.* 2002; Migeon *et al.* 2010) (Fig. 4). The identification of a palaeochannel in the upslope domain, combined with core observations, indicates that the Unit III deposits are most likely to have been transported and deposited by turbidity currents through that channel, creating levees and extending broadly into the Tuaheni Basin. The increased thickness of Unit III within the channel thalweg could be explained by a backfilling and subsequent abandonment of the channel (e.g. Cronin *et al.* 2005; Dalla Valle & Gamberi 2011).

Unit III presents various seismic facies within the surveyed area, with the most prevalent one being a chaotic to transparent facies. This type of facies is usually interpreted as deformed material, mixed debris, MTDs, etc. (Bull *et al.* 2009). Another type of facies in Unit III is the sub-parallel stratified facies (Fig. 3), that is likely to correspond to undisturbed strata either *in situ* and undeformed, or translated with minimal or no deformation. The round low-variance patches observable on variance slices (Fig. 7b) seem to coincide with the packages of parallel reflectors and could correspond to blocks (Gamboa & Alves 2015). In core U1517C, the deposits do not appear to have undergone major deformation, and the sedimentary sequence at this precise location could correspond to one

of these blocks. Unit III presents a chaotic seismic facies at the location where the core was drilled. However, despite the high resolution of the data, blocks under 5 m in diameter are unlikely to be detected. More blocks have been identified throughout the volume based on observation of sharply contrasted zones in variance slices. We suggest that the presence of blocks within Unit III shows that the unit was remobilized after deposition. Seismic data analysis shows that the Tuaheni Canyon south of the TLC, visible on bathymetry data and thought to be a vector of material removal (Mountjoy *et al.* 2009), already existed at the time Unit III was emplaced. Considering that the conveyor belt model proposed by Mountjoy *et al.* (2009) was already active at that time, we propose that Unit III was subject to a continuous loss of support downslope, that induced the lateral spreading of its sedimentary sequences, creating an extensional system similar to what is observed in the Gulf of Mexico (Sawyer *et al.* 2009), with blocks being pulled away from each other, slowly becoming surrounded by debris depositing *in situ*. On land, an analogue to this mechanism could be peat flows in Irish bogs: peat landslides can form a system of 'rafts' carried by liquefied peat and debris-filled troughs (Dykes & Warburton 2007). Similar onland analogues, in which lateral spread in clay induces displacement of blocks, forming systems of horsts and grabens, were observed in North America (Hungr *et al.* 2014). This emplacement mechanism could explain how Unit III can present a chaotic facies in places and parallel reflections in others, and how in core U1517C little deformation is observable.

Unit II emplacement model

Landslide kinematic indicators (onshore and offshore alike) generally show extension upslope due to sediment depletion and an area of compression downslope due to debris accumulation (Glastonbury & Fell 2008). In the case of the TLC, the mechanics of the landslide differ, as 3D seismic data show that compression occurred in the upslope domain and shows arcuate concave ridges that are evidence of extension in the downslope domain of Lobe T2. These observations concur with previous analysis of bathymetry data at the TLC (Mountjoy *et al.* 2009).

The geometry of the central ridge reflectors on seismic data indicates that the central ridge sedimentary sequence deposited before the emplacement of the Unit II MTD. Using 3D seismic data and attribute analysis, we identified dip-slip gravitational faults at the sides of the central ridge and at the edges of large-scale blocks northwest of the central ridge (Figs 3, 5 & 7a), suggesting that the central ridge is the remainder of a larger sedimentary sequence, which partly collapsed. The geometry and internal seismic architecture of the central ridge is indicative of a contouritic deposit (Rebesco *et al.* 2014). Therefore, we propose that Unit II was sourced from a mix of lowstand systems tract sediments that occupied the upslope area (Mountjoy *et al.* 2009) and of coutouritic deposits accumulated in the mid-slope area, which collapsed locally as a result of a loss of support downslope induced by the continuous removal of material in the distal domain, due to the presence of the Tuaheni Canyon (conveyor belt model) (Mountjoy *et al.* 2009). Evidence for this is provided by the extensional faults forming concave upwards arcuate ridges in the evacuation channel downslope, in the upper reaches of the Tuaheni Canyon (Figs 3 & 8a). We stress that it remains ambiguous whether the deformation features in the TLC represent active creeping (as proposed by Mountjoy *et al.* (2009)) or whether the landslide complex was reactivated only once in the past and is now immobile.

Proposed sequence of events

We interpret that Unit III was first deposited on top of previously faulted pre-slide Quaternary clinoforms (Gross *et al.* 2018) by turbidity currents, via at least one channel, forming a deep sea fan (Fig. 10a). That channel is likely to have backfilled and then been abandoned, possibly due to a relocation of the channel. Removal of material downslope through the Tuaheni Canyon, caused these fan deposits to spread laterally, forming rounded blocks between which debris was in-filled (Fig. 10b). The sedimentary sequence equivalent to the central ridge was then deposited, possibly due to the activity of bottom currents and/or advance of the Quaternary lowstand systems tract on the slope (Fig. 10c & 10d). Very little is known about contourite deposits anywhere on the Hikurangi Margin continental slope, making unequivocal identification of the central ridge as a contourite difficult. The remainder of these sequences lie north of Lobe T3, between Tuaheni North and Tuaheni South. The rest failed, and became the Tuaheni Landslide Complex, due to loss of downslope support, as material continued to get evacuated through the Tuaheni Canyon (Fig. 10e). Gravitational faults and blocks developed and left only the contourite deposits of the central ridge unaffected. Unit I, which is a thin drape of hemipelagites at U1517C, but possibly more variable at its upslope extent, was then deposited on top of the debris, filling the lows created by the displacement of blocks in Unit II. In our proposed depositional model, Unit II and Unit III have different sources and different emplacement mechanisms. We interpret that the only thing that the units have in common is the cause for failure, i.e. the presence of the Tuaheni Canyon that likely causes constant extension on the deposits on the slope. This new depositional model contrasts with the previous model (Mountjoy *et al.* 2014), which had interpreted the lower unit to be a parent unit to the upper one.

Conclusions

Interpretation of 3D seismic data and analysis of 3D seismic attributes, combined with newly acquired sedimentary information from IODP Expedition 372 (core U1517C), have allowed a better understanding of the geometry and morphology of the TLC units previously known as the lower and upper landslide units. A key result in understanding the lateral extent of Unit III comes from the calculation of the variance attribute from an arbitrary level (at an offset from horizon R4) within the interpreted body of Unit III (Fig. 7b). It is clear that the broad character of the unit extends through the sub-surface region of the central ridge (Fig. 7b). By contrast, if we extend an arbitrary surface from within Unit II through the central ridge, we observe a marked change in the variance attribute beneath the central ridge. These two maps (Fig. 7) demonstrate that Unit II is bounded by relatively coherent (i.e. well stratified, low seismic variance) strata of the central ridge, while Unit III likely continues laterally beneath the central ridge. This means that Unit III was deposited prior to the formation of the central ridge. We find that these two units (II and III; corresponding to upper and lower, respectively), defined in core U1517C during IODP Expedition 372 and correlated with seismic data thereafter, have distinct emplacement mechanisms and are not genetically linked. The source of the debris and the deformation processes differ. Hence, the status of Unit III being a part of the TLC should be reconsidered as the proposed sequence of events implies that between Units II and III there is a significant time interval, although it is hard to estimate how long in this study. From these findings, we propose a new depositional model and emplacement history for the TLC. The presence of the Tuaheni Canyon in the downslope extent of both units is significant as it enabled lateral spreading by removal of frontal support. Whether its effect on the slope deposits causes continuous creeping movement of the TLC or whether this happened suddenly remains ambiguous. Considering the results presented in this paper, future research should focus on the geomechanics at the R2

horizon that separates Unit II from Unit III, as it is likely the basal shear surface of the TLC and if there is creeping movement this is where it is most likely focused.

Acknowledgements The authors thank the IODP Expedition 372 crew and participants and the expedition staff scientist Dr Leah Levay. We are grateful to the shipboard party of IODP Exp 372 for all the onboard efforts and valuable discussions regarding the Tuaheni Landslides. Prof Ann Cook and Prof Derek Sawyer at Ohio State University are thanked for providing access to their laboratory facilities. Thanks to Dr Eoin Dunlevy for his valuable technical assistance regarding the use of seismic interpretation software. Finally, we thank Dr Matthew J. Owen and Dr Jaume Llopart for their careful reviews, which helped improve greatly the quality of this work.

Funding This publication has emanated from research supported by a research grant from Science Foundation Ireland (SFI) under Grant Number 17/RC-PhD/3481 and is co-funded under the European Regional Development Fund.

Georgiopoulou received funding support by the Geological Survey Ireland to participate on IODP Expedition 372. Mountjoy and Crutchley are funded by the Royal Society of New Zealand Marsden Fund Grant NIW1603.

We thank the crew and participants of TAN1404. The collection and processing of the P-Cable 3D volume was jointly funded by the New Zealand Ministry for Business Innovation and Employment (MBIE), NIWA and GNS Science SSIF funding and the Deutsche Forschungsgemeinschaft (DFG-Grant BI 404/7 | KR 2222/18). The collection and processing of multibeam data was funded by NIWA SSIF.

References

Anderson, H., & Webb, T. (1994). New Zealand seismicity: Patterns revealed by the upgraded National Seismograph Network. *New Zealand Journal of Geology and Geophysics*, **37** (4), 477–493. https://doi.org/10.1080/00288306.1994.9514633

Babonneau, N., Savoye, B., Cremer, M., & Klein, B. (2002). Morphology and architecture of the present canyon and channel system of the Zaire deep-sea fan. *Marine and Petroleum Geology*, **19** (4), 445–467. https://doi.org/10.1016/S0264-8172(02)00009-0

Böttner, C., Gross, F., Geersen, J., Crutchley, G. J., Mountjoy, J. J., & Krastel, S. (2018). Marine Forearc Extension in the Hikurangi Margin: New Insights From High-Resolution 3-D Seismic Data. *Tectonics*, **37** (5), 1472–1491. https://doi.org/10.1029/2017TC004906

Bull, S., Cartwright, J., & Huuse, M. (2009). A review of kinematic indicators from mass-transport complexes using 3D seismic data. *Marine and Petroleum Geology*, **26** (7), 1132–1151. https://doi.org/10.1016/j.marpetgeo.2008.09.011

Chiswell, S. M., Bostock, H. C., Sutton, P. J. H., & Williams, M. J. (2015). Physical oceanography of the deep seas around New Zealand: A review. *New Zealand Journal of Marine and Freshwater Research*, **49** (2), 286–317. https://doi.org/10.1080/00288330.2014.992918

Cronin, B. T., Akhmetzhanov, A. M., Mazzini, A., Akhmanov, G., Ivanov, M., & Kenyon, N. H. (2005). Morphology, evolution and fill: Implications for sand and mud distribution in filling deep-water canyons and slope channel complexes. *Sedimentary Geology*, **179** (1–2), 71–97. https://doi.org/10.1016/j.sedgeo.2005.04.013

Dalla Valle, G., & Gamberi, F. (2011). Slope channel formation, evolution and backfilling in a wide shelf, passive continental margin (northeastern sardinia slope, central tyrrhenian sea). *Marine Geology*, **286** (1–4), 95–105. https://doi.org/10.1016/j.margeo.2011.06.005

Dykes, A. P., & Warburton, J. (2007). Mass movements in peat: A formal classification scheme. *Geomorphology*, **86** (1–2), 73–93. https://doi.org/10.1016/j.geomorph.2006.08.009

Fruergaard, M., Piasecki, S., Johannessen, P. N., Noe-Nygaard, N., Andersen, T. J., Pejrup, M., & Nielsen, L. H. (2015). Tsunami propagation over a wide, shallow continental shelf caused by the Storegga slide, southeastern North Sea, Denmark. *Geology*, **43** (12), 1047–1050. https://doi.org/10.1130/G37151.1

Gamboa, D., & Alves, T. M. (2015). Three-dimensional fault meshes and multi-layer shear in mass-transport blocks: Implications for fluid flow on continental margins. *Tectonophysics*, **647**, 21–32. https://doi.org/10.1016/j.tecto.2015.02.007

Gee, M. J. R., & Gawthorpe, R. L. (2007). Early evolution of submarine channels offshore Angola revealed by three-dimensional seismic data. *Geological Society Special Publication*, **277**, 223–235. https://doi.org/10.1144/GSL.SP.2007.277.01.13

Glastonbury, J., & Fell, R. (2008). Geotechnical characteristics of large slow, very slow, and extremely slow landslides. *Canadian Geotechnical Journal*, **45** (7), 984–1005. https://doi.org/10.1139/T08-021

Gross, F., Mountjoy, J. J., Crutchley, G. J., Böttner, C., Koch, S., Bialas, J., … Krastel, S. (2018). Free gas distribution and basal shear zone development in a subaqueous landslide – Insight from 3D seismic imaging of the Tuaheni Landslide Complex, New Zealand. *Earth and Planetary Science Letters*, **502**, 231–243. https://doi.org/10.1016/J.EPSL.2018.09.002

Hampton, M. a., Lee, H. J., & Locat, J. (1996). Submarine landslides. *Geophysics*, **34** (1), 33–59. https://doi.org/10.1029/95rg03287

Hungr, O., Leroueil, S., & Picarelli, L. (2014). The Varnes classification of landslide types, an update. *Landslides*, **11** (2), 167–194. https://doi.org/10.1007/s10346-013-0436-y

Ioualalen, M., Migeon, S., & Sardoux, O. (2010). Landslide tsunami vulnerability in the Ligurian Sea: Case study of the 1979 October 16 Nice international airport submarine landslide and of identified geological mass failures. *Geophysical Journal International*, **181** (2), 724–740. https://doi.org/10.1111/j.1365-246X.2010.04572.x

Kelner, M., Migeon, S., Tric, E., Couboulex, F., Dano, A., Lebourg, T., & Taboada, A. (2016). Frequency and triggering of small-scale submarine landslides on decadal timescales: Analysis of 4D bathymetric data from the continental slope offshore Nice (France). *Marine Geology*, **379**, 281–297. https://doi.org/10.1016/j.margeo.2016.06.009

Koson *et al.* 2014. Seismic attributes and seismic geomorphology. *Bulletin of Earth Sciences of Thailand*; Vol. **6**, No. 1, 1-9

Kuhlmann, J., Orpin, A. R., Mountjoy, J. J., Crutchley, G. J., Henrys, S., Lunenburg, R., & Huhn, K. (2018). Seismic and lithofacies characterization of a gravity core transect down the submarine Tuaheni Landslide Complex, NE New Zealand. *Geological Society, London, Special Publications*, SP477.**37**. https://doi.org/10.1144/sp477.37

Migeon, S., Ducassou, E., Le Gonidec, Y., Rouillard, P., Mascle, J., & Revel-Rolland, M. (2010). Lobe construction and sand/mud segregation by turbidity currents and debris

flows on the western Nile deep-sea fan (Eastern Mediterranean). *Sedimentary Geology*, **229** (3), 124–143. https://doi.org/10.1016/j.sedgeo.2010.02.011

Mountjoy, J. J., McKean, J., Barnes, P. M., & Pettinga, J. R. (2009). Terrestrial-style slow-moving earthflow kinematics in a submarine landslide complex. *Marine Geology*, **267** (3–4), 114–127. https://doi.org/10.1016/j.margeo.2009.09.007

Mountjoy, J. J., Pecher, I., Henrys, S., Crutchley, G., Barnes, P. M., & Plaza-Faverola, A. (2014). Shallow methane hydrate system controls ongoing, downslope sediment transport in a low-velocity active submarine landslide complex, Hikurangi Margin, New Zealand. *Geochemistry, Geophysics, Geosystems*, **15** (11), 4137–4156. https://doi.org/10.1002/2014GC005379

Mulder, T., & Cochonat, P. (1996). Classification of Offshore Mass Movements. *SEPM Journal of Sedimentary Research, Vol.* **66**, 43–57. https://doi.org/10.1306/D42682AC-2B26-11D7-8648000102C1865D

Newnham, R. M., Lowe, D. J., & Williams, P. W. (1999). Quaternary environmental change in New Zealand: a review. *Progress in Physical Geography: Earth and Environment*, **23** (4), 567–610. https://doi.org/10.1177/030913339902300406

Paquet, F., Proust, J.-N., Barnes, P. M., & Pettinga, J. R. (2009). Inner-Forearc Sequence Architecture in Response to Climatic and Tectonic Forcing Since 150 ka: Hawke's Bay, New Zealand. *Journal of Sedimentary Research*, **79** (3), 97–124. doi:10.2110/jsr.2009.019

Pecher, I. A., Barnes, P. M., Levay, L. J., & Scientists, E. (2018). Expedition 372 Preliminary Report Creeping Gas Hydrate Slides and Hikurangi LWD, (November 2017).

Pedley, K. L., Barnes, P. M., Pettinga, J. R., & Lewis, K. B. (2010). Seafloor structural geomorphic evolution of the accretionary frontal wedge in response to seamount subduction, Poverty Indentation, New Zealand. *Marine Geology*, **270** (1–4), 119–138. https://doi.org/10.1016/j.margeo.2009.11.006

Piper, D. J. W., Cochonat, P., & Morrison, M. L. (1999). The sequence of events around the epicentre of the 1929 Grand Banks earthquake: Initiation of debris flows and turbidity current inferred from sidescan sonar. *Sedimentology (1999)* **46**, 79–97.

Randen T., Sønneland L. (2005) Atlas of 3D Seismic Attributes. In: Iske A., Randen T. (eds) Mathematical Methods and Modelling in Hydrocarbon Exploration and Production. Mathematics in Industry, vol **7**. Springer, Berlin, Heidelberg

Rebesco, M., Hernández-molina, F. J., Rooij, D. Van, & Wåhlin, A. (2014). Contourites and associated sediments controlled by deep-water circulation processes : State-of-the-art and future considerations. *Marine Geology*, **352**, 111–154. https://doi.org/10.1016/j.margeo.2014.03.011

Sawyer, D. E., Flemings, P. B., Dugan, B., & Germaine, J. T. (2009). *Retrogressive failures recorded in mass transport deposits in the Ursa Basin , Northern Gulf of Mexico*. **114** (July), 1–20. https://doi.org/10.1029/2008JB006159

Talling, P. J., Paull, C. K., & Piper, D. J. W. (2013). How are subaqueous sediment density flows triggered, what is their internal structure and how does it evolve? Direct observations from monitoring of active flows. *Earth-Science Reviews*, **125**, 244–287. https://doi.org/10.1016/j.earscirev.2013.07.005

Wallace, L. M., Beavan, J., McCaffrey, R., & Darby, D. (2004). Subduction zone coupling and tectonic block rotations in the North Island, New Zealand. *Journal of Geophysical Research: Solid Earth*, **109** (12), 1–21. https://doi.org/10.1029/2004JB003241

Wright, I., McGlone, M., Nelson, C., & Pillans, B. (1995). An Integrated Latest Quaternary (Stage 3 to Present) Paleoclimatic and Paleoceanographic Record from Offshore Northern New Zealand. *Quaternary Research,* **44** (2), 283-293. doi:10.1006/qres.1995.1073

Figure captions

Fig. 1. (**a**) Map of New Zealand and surrounding bathymetry showing the location of the Hikurangi margin and the study area (white box). Courtesy of NIWA. (**b**) Enlarged view of the study area with shaded relief bathymetry, showing the 3D seismic survey area in pink, as well as the location of the TLC South lobes (after Mountjoy *et al.* 2009), the IODP core site (U1517) and the three composite seismic lines shown in this study.

Fig. 2. (**a**) Interpreted sedimentary log of the upper part of IODP core U1517C, drilled during Exp 372. Left: Interpretation of sedimentary facies identified within Units I to III. Right: Interpreted photographs of representative sections of the core. Facies number is indicated in the upper left corner of each photograph. Core section number is indicated on the left side of each photograph. (**b**) Grain size measurements from sections 1H-4W (Unit II) and 11F-4W (Unit III) of IODP core U1517C.

Fig. 3. Seismic line extracted from 3D seismic volume SCHLIP-3D acquired during expedition TAN1404 (Inline XX'). (**a**) Uninterpreted seismic data. (**b**) Enlarged view of the block NW of the central ridge. Magnification from inline XX' (**c**) Enlarged view of the small-size blocks visible on inline XX' (**d**) Interpretation of inline XX'.

Fig. 4. Seismic line extracted from 3D seismic volume SCHLIP-3D acquired during expedition TAN1404 (Crossline YY'). (**a**) Uninterpreted seismic data. (b) Interpretation of crossline YY'.

Fig. 5. Seismic line extracted from 3D seismic volume SCHLIP-3D acquired during expedition TAN1404 (Crossline ZZ'). (**a**) Uninterpreted seismic data. (**b**) Interpretation of crossline ZZ'.

Fig. 6. Horizon R2, corresponding to the base of Unit II. (**a**) 3D view of the base surface of Unit II. The white arrows represent flow directions. (**b**)Two-way time map of Unit II in ms. (**c**) 3D representation of the gradient attribute applied to Reflector R2. The red colour shows the low angle slopes, whereas the blue represents the steepest slopes. (**d**) Gradient map of the base of Unit II.

Fig. 7. Variance maps of Unit II and Unit III in time (ms), using the variance attribute. (**a**) Variance map of Reflector R3+20 ms (above Unit III). This map shows how Unit II and the central ridge sequence have distinctly different seismic facies. (**b**) Variance map of Reflector R4+20 ms (within Unit III). This map shows the dislocated state of the Unit III sedimentary package. White patches correspond to a block of parallel seismic facies, around which the seismic facies is chaotic to transparent (in black).

Fig. 8. Thickness maps of Unit II and Unit III in time (ms). (**a**) Thickness map of Unit II. (**b**) Thickness map of Unit III.

Fig. 9. Horizon R4, corresponding to the base of Unit III. (**a**) 3D view of the base surface of Unit III. The white arrows represent interpreted flow directions. Note the dashed lines representing interpreted secondary flow directions (levees). (**b**) Two-way time (TWT) map of Unit III in ms. (**c**) 3D representation of the gradient attribute applied to Reflector R4. (**d**) Gradient map of the base of Unit III using the dip angle attribute. The thick dashed arrows indicate the source of sediment influx.

Fig. 10. A new depositional model for the Tuaheni Landslide Complex, proposed from interpretation of seismic data and sediment core. Note: the mid blue colour in (e) represents landslide material that flow around the central ridge, not beneath it.

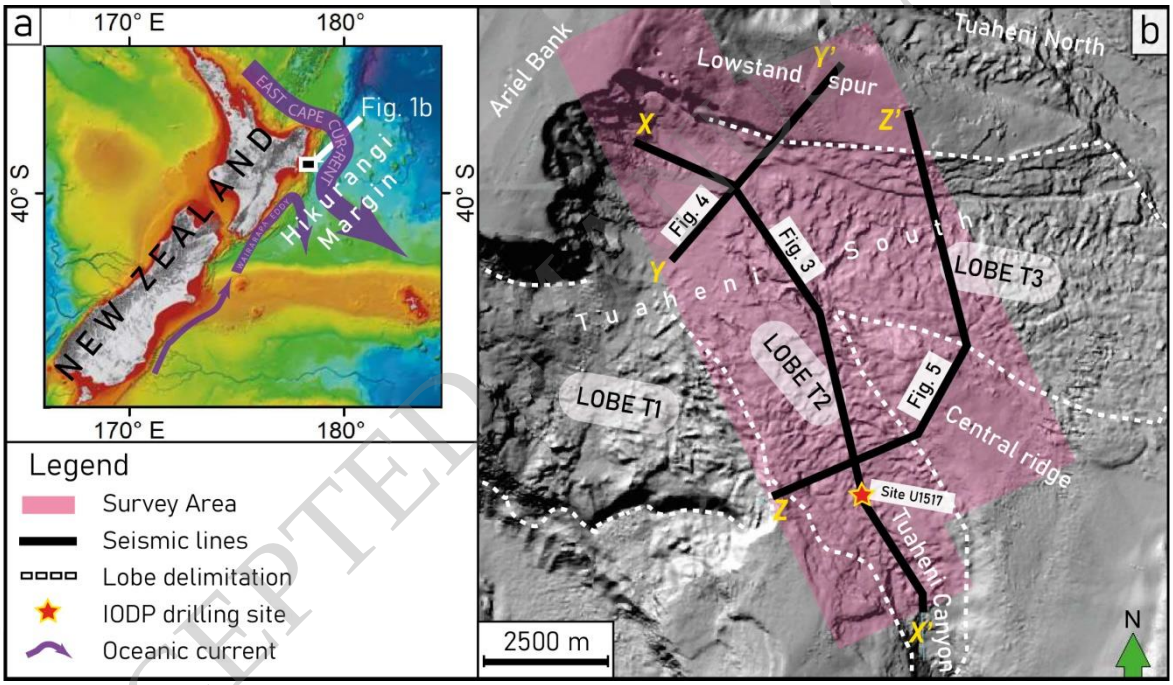

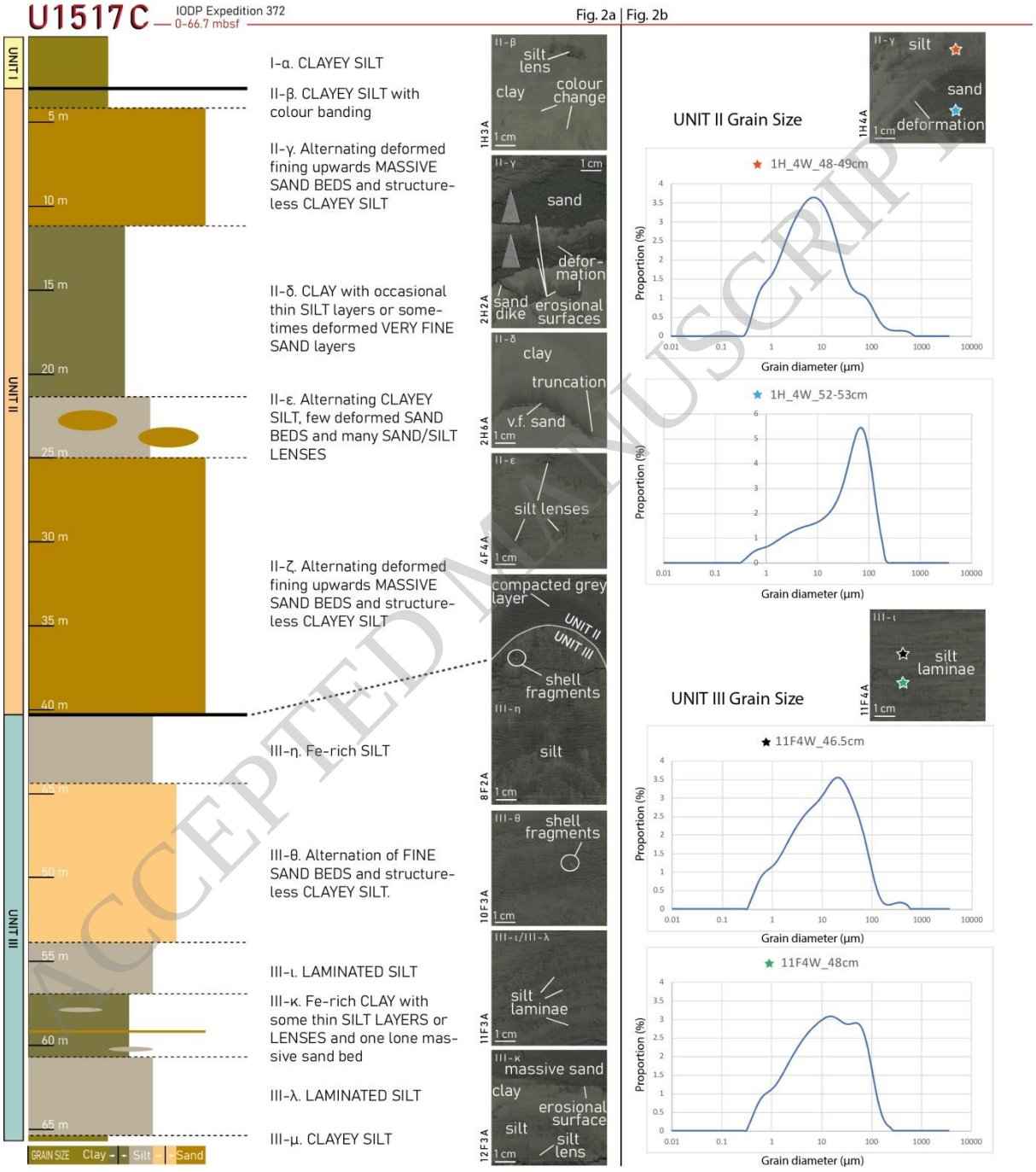

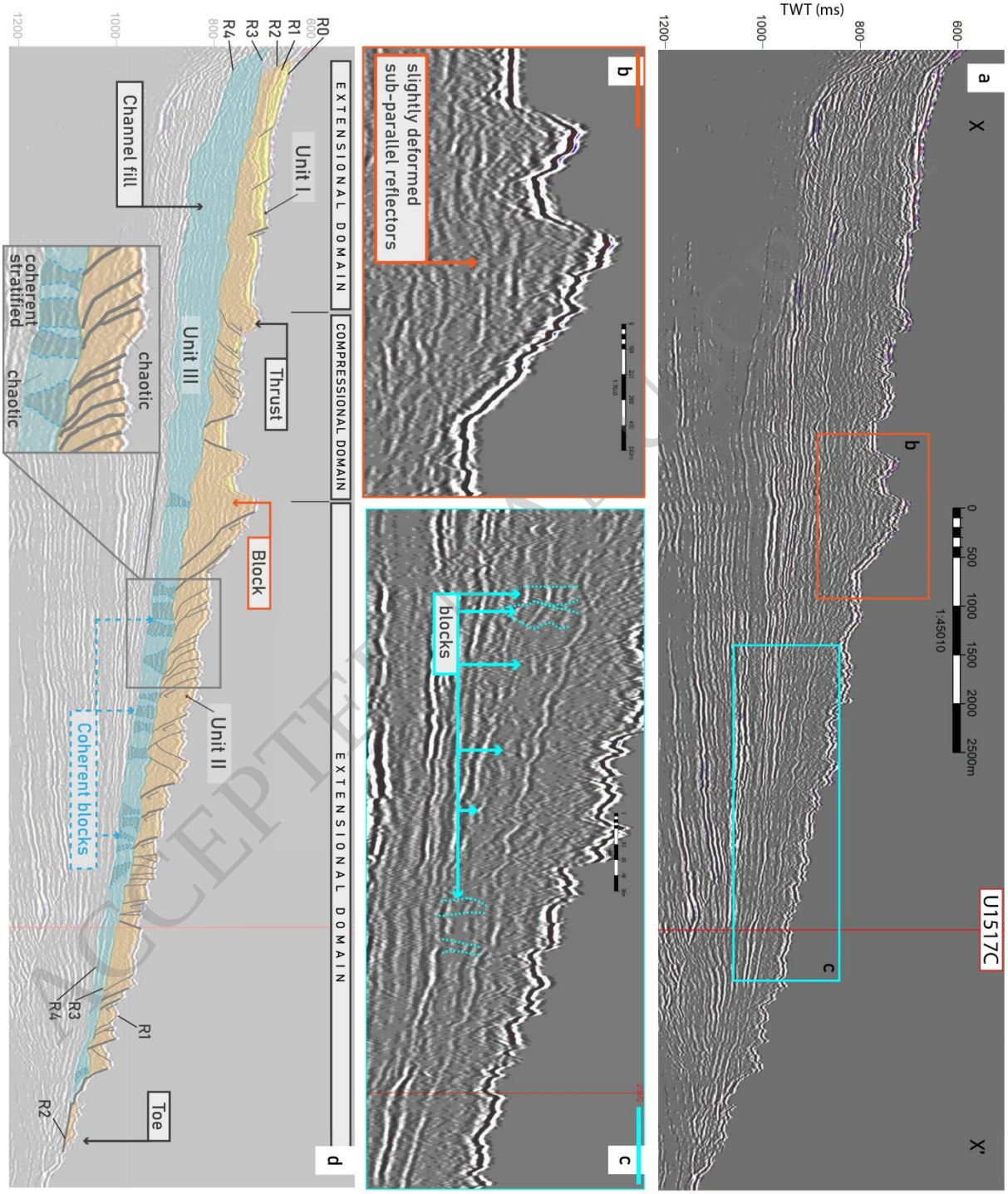

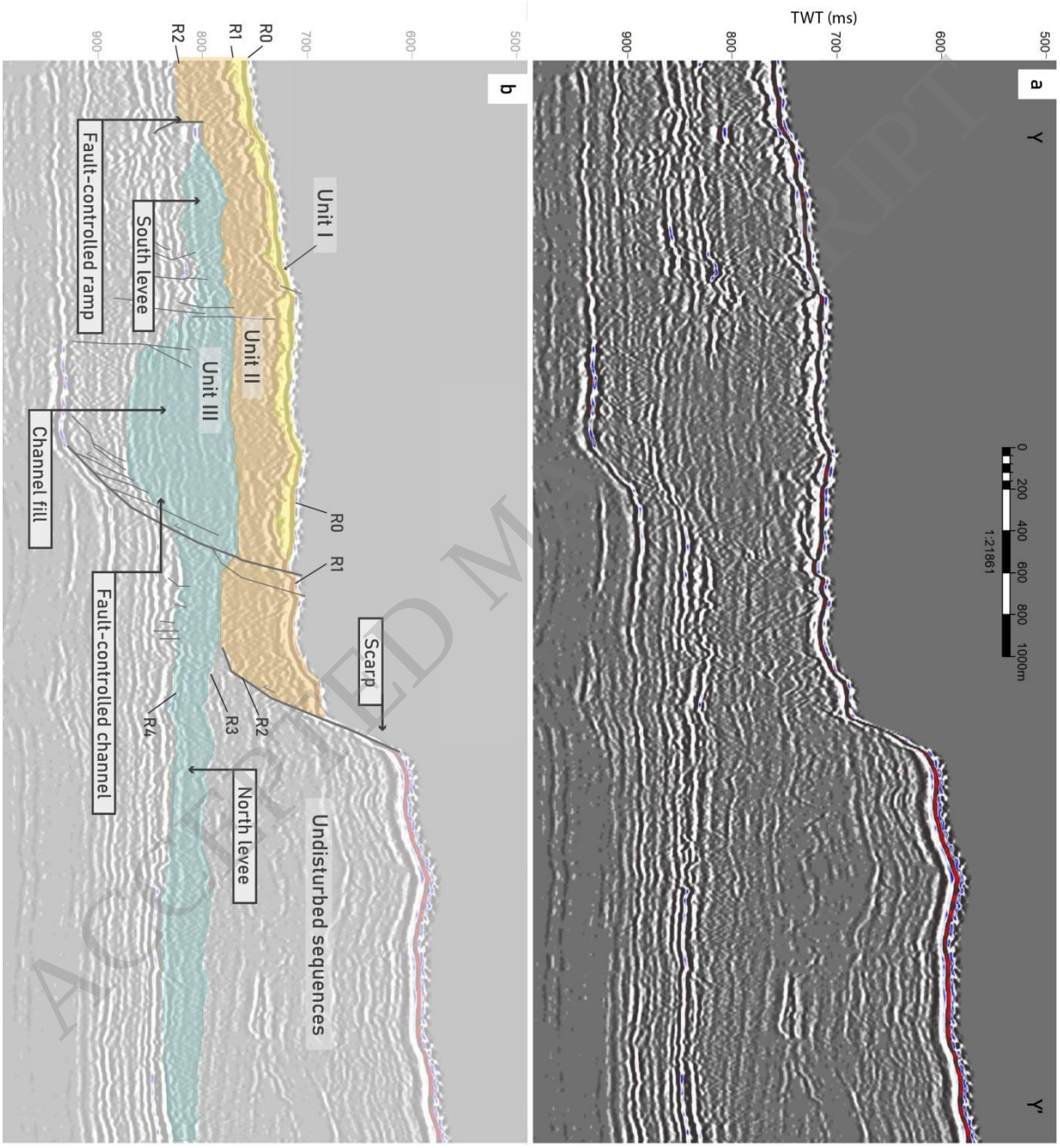

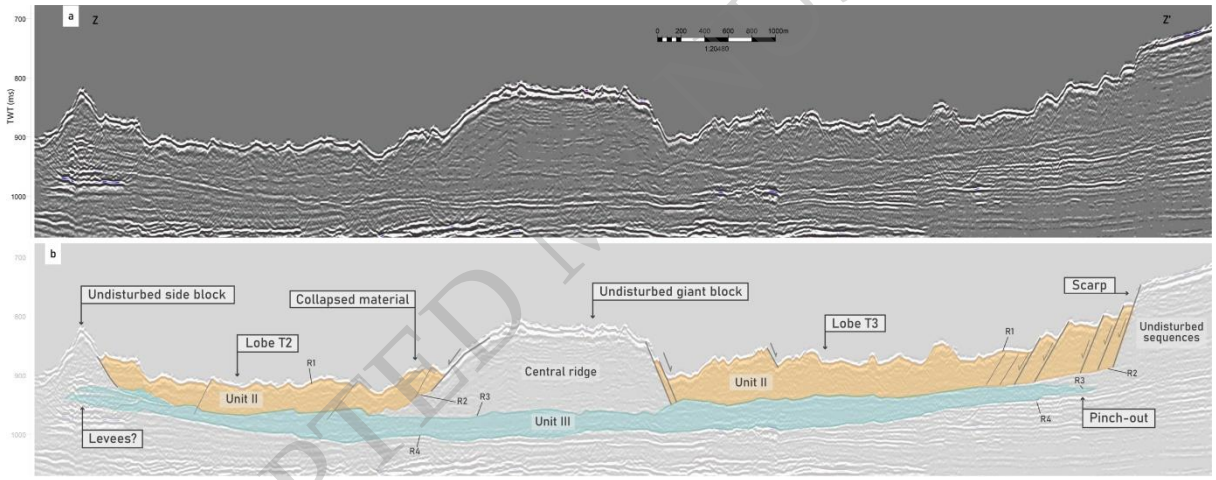

Horizon R2 (Base Unit II)

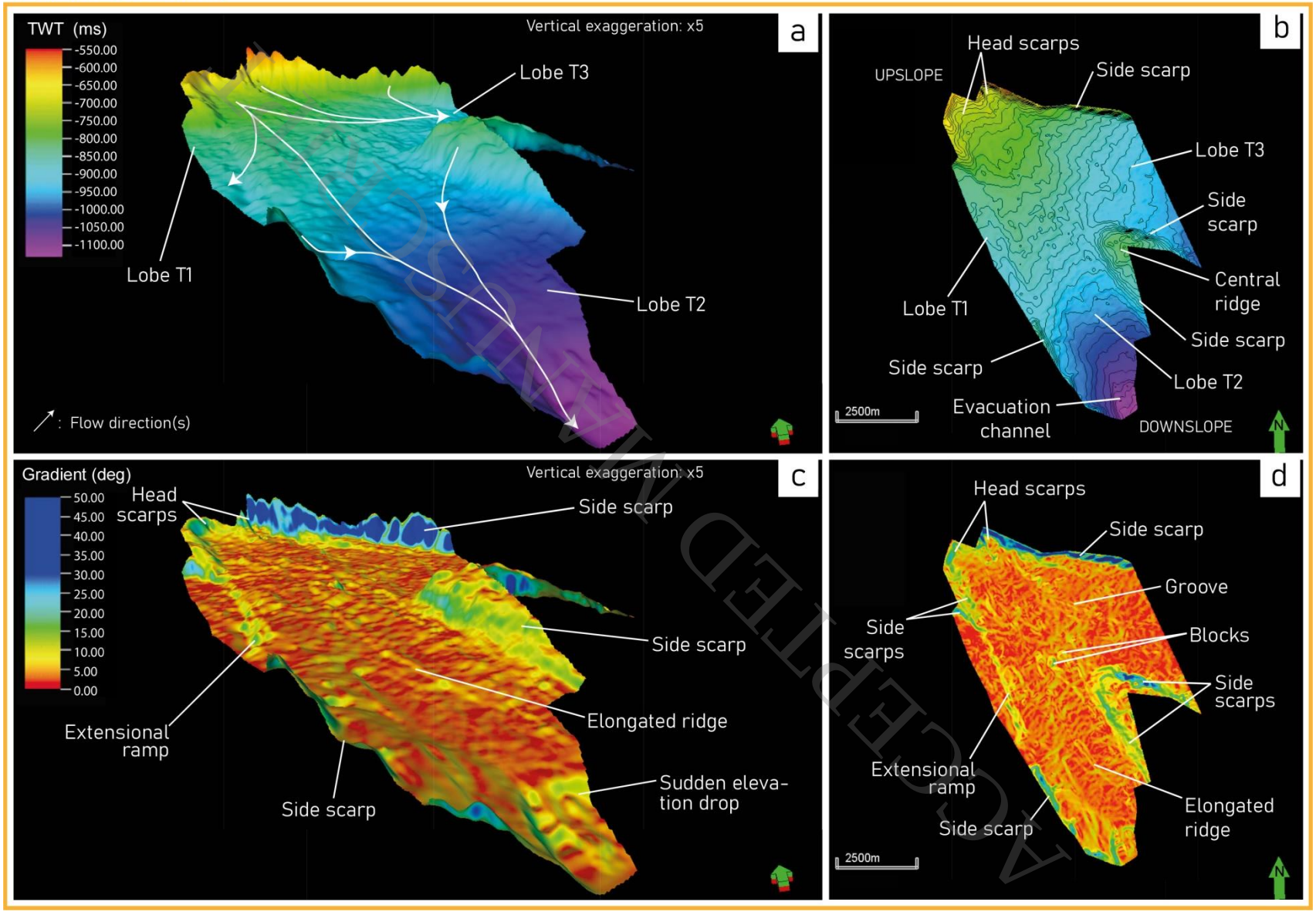

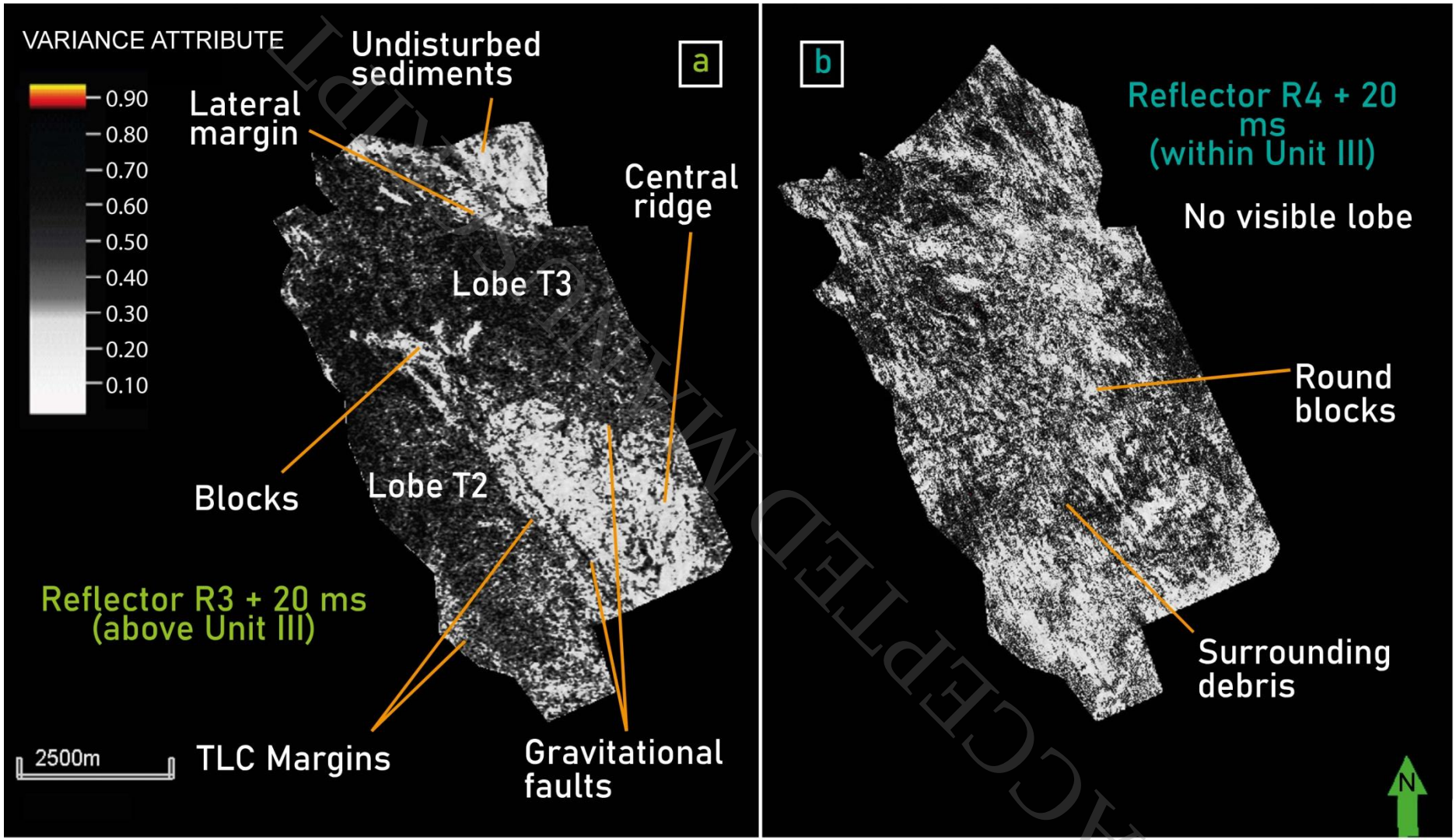

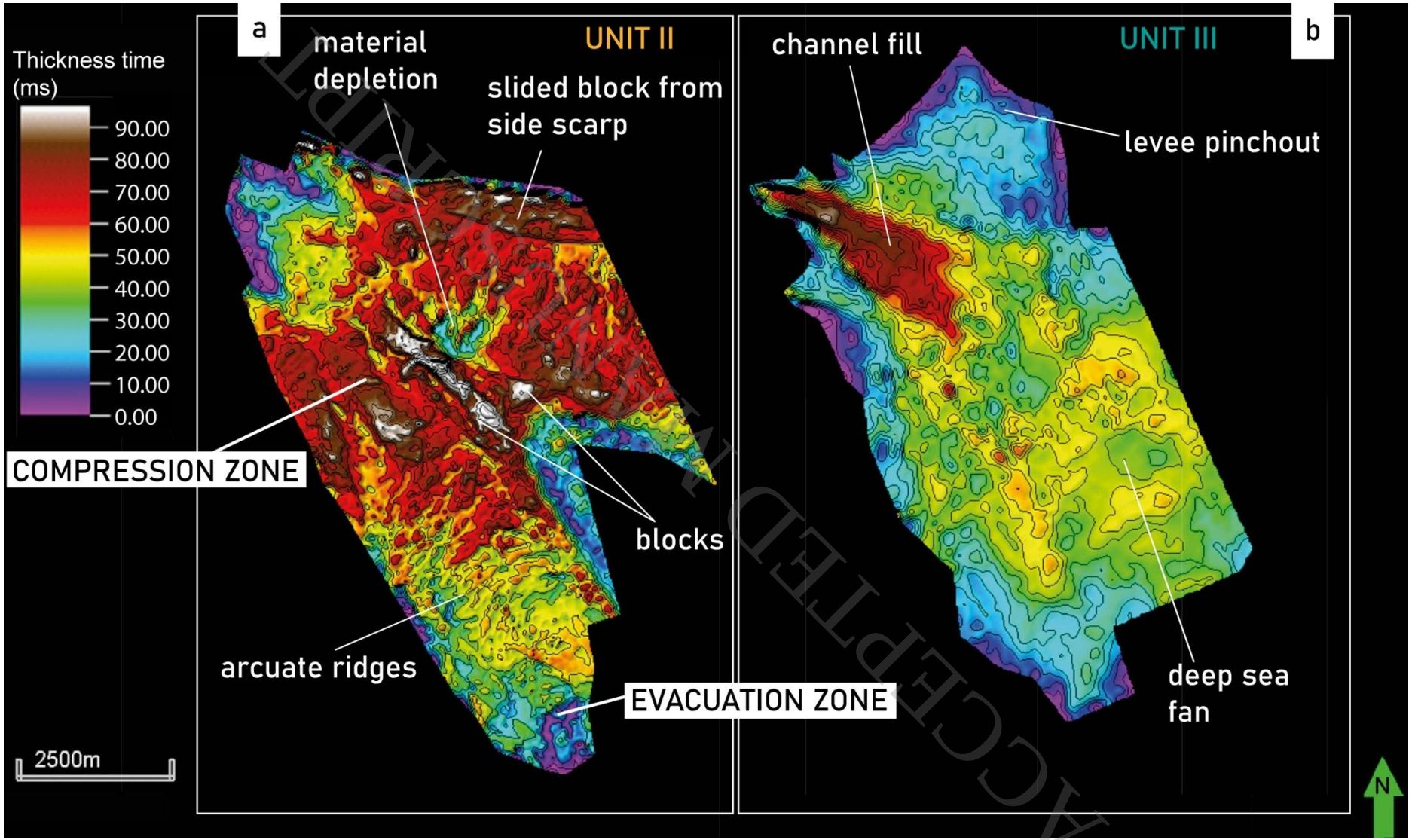

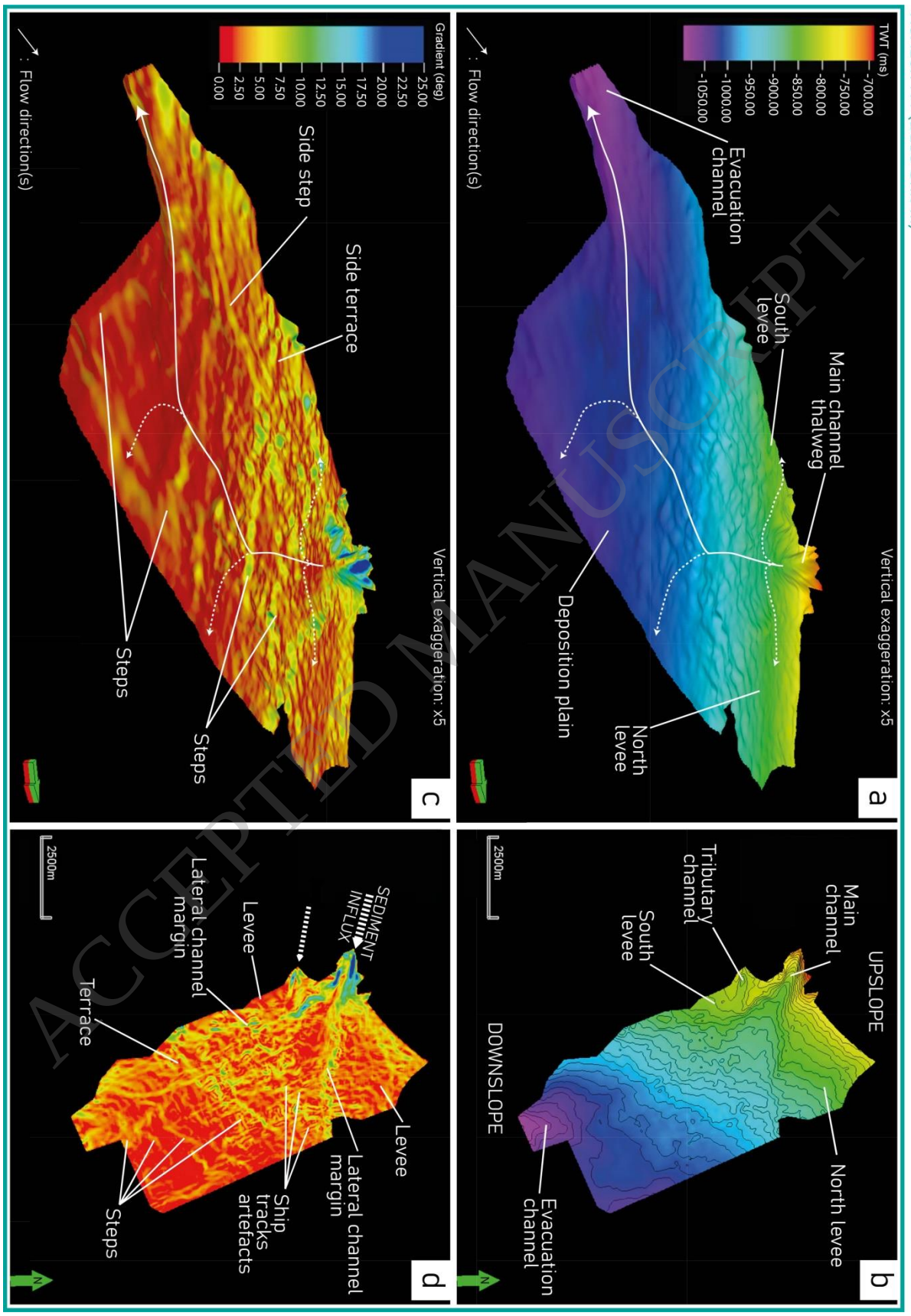

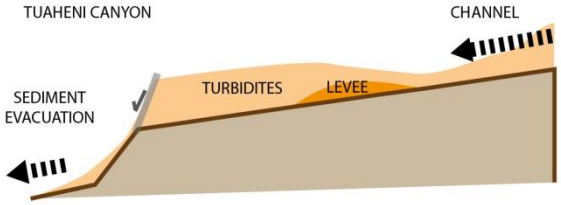

(a) Turbidites are deposited onto the Tuaheni Basin via a channel, creating levees on the sides of the channel. Sediment starts getting evacuated through the pre-existing Tuaheni Canyon.

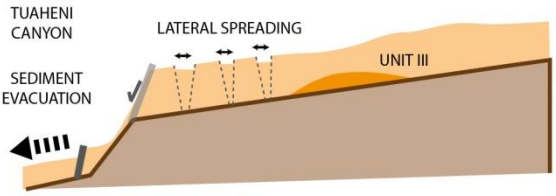

(b) Evacuation of material induces lateral spreading of silty deposits. A system of blocks surrounded by debris is progressively formed.

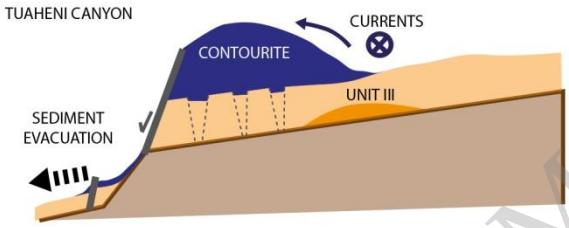

(c) The upslope channel gets backfilled and dies, while coutourites are deposited, forming a wedge.

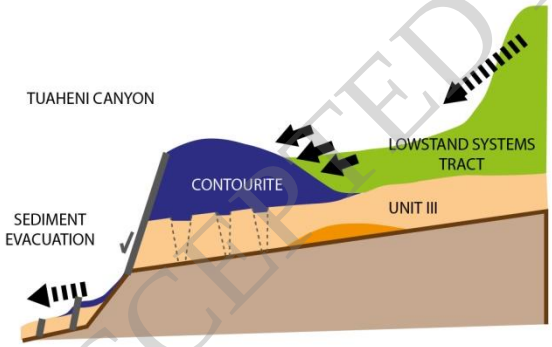

(d) High influx of sediments fill the basin, forming a progradating lowstand systems tract, as material continues to get evacuated through the Tuaheni Canyon.

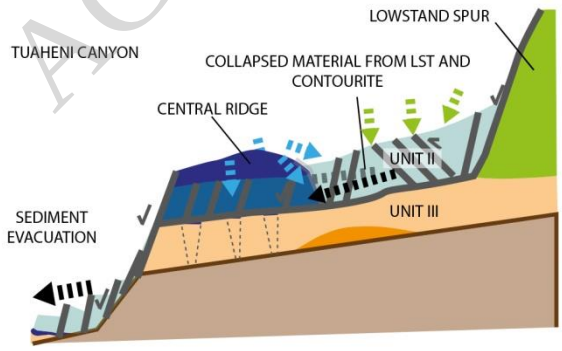

(e) The unstable system collapses, as material sourcing from the lowstand systems tract and the contourite deposits start flowing toward the Tuaheni basin.